Analyst

ROYAL SOCIETY OF CHEMISTRY

COMMUNICATION

View Article Online
View Journal | View Issue

Cite this: *Analyst*, 2022, **147**, 1071

Received 3rd December 2021,
Accepted 2nd February 2022

DOI: 10.1039/d1an02190g

rsc.li/analyst

Conducting and characterizing femto flow electrospray ionization†

Huishan Li, Nicholas Allen, Mengtian Li and Anyin Li *

Femto flow electrospray ionization (ESI) with flow rates ranging from 240 fL min^{-1} to the low pico level (<10 pL min^{-1}) was conducted and measured using a submicron emitter tip and relay ESI configuration. Signature analyte ion current intensities and profiles were observed. The obtained flow rate and ionization current enabled size calculation for initial charged nanodroplets.

Electrospray ionization (ESI) is a widely used method in mass spectrometry[1] and surface modification.[2] The flow rate is a key parameter of ESI as it correlates with the size of the produced initial charged droplets.[3] Smaller initial charged droplets exhibit enhanced performances such as improved ionization efficiency, reduced nonspecific adduct formation, and lower sample consumption.[4–6] Reducing the flow rate for ESI is a continuing research direction with lower limits being reported for micrometer emitter tips in the range of 30–300 pL min^{-1}.[7–9]

Since their first introduction by Baker *et al.*,[4] submicron emitter tips have attracted growing attention in ESI mass spectrometry. The smaller initial charged droplets produced by the submicron emitter tips effectively reduce nonspecific adducts and salt clusters,[10,11] which is critical for the analysis of native biomolecules and complexes.[5,12–14] However, except for the 26 pL min^{-1} flow rate for a 600 nm emitter tip,[15] the flow rates for most submicron emitter tips are unknown. Femtoamp electrospray ionization (fA ESI) was developed using both micrometer and submicron emitter tips.[16] The observed MS intensities, being 2–3 orders of magnitude lower than those produced by 50 pL min^{-1} ESI,[17] suggest that the flow rates for these emitter tips could be in the femto range. These new findings bring challenges and exciting opportunities for characterizing and further developing low flow electrospray ionization.

Here we present the instrument methods for conducting and characterizing ultra-low ESI with flow rates <10 pL min^{-1}. As shown in Fig. 1, a thin long tapered submicron emitter tip was adopted to track volume changes as small as 3 fL. Loading *ca.* 10 pL aqueous solution (Fig. S1†) creates two air–liquid interfaces, one at the submicron tip opening and another at the back end with a μm-sized diameter. These two interfaces had a combined evaporation rate of tens of picoliters per minute under typical lab conditions. As evaporation is determined by the air–liquid interface (Table S1 and Fig. S2†),

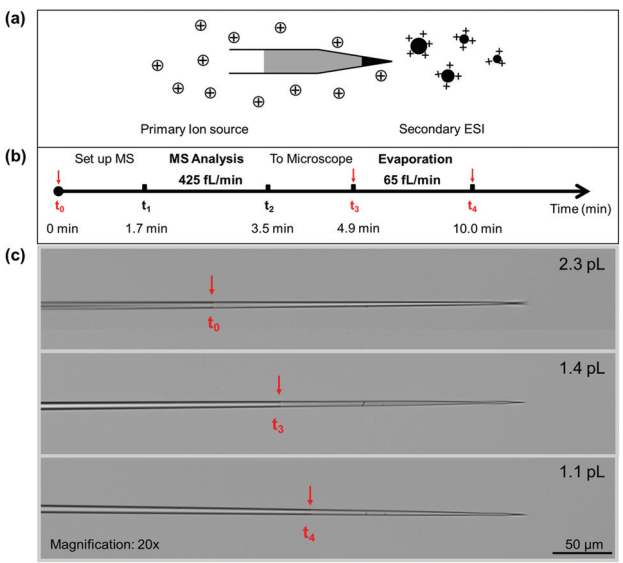

Fig. 1 Conducting and measuring femto flow electrospray ionization mass spectrometry. (a) Scheme of the relay ESI setup. The sample solution (black) in the secondary emitter was ionized by electrospray triggered by charges from a primary ion source. In the secondary emitter, a hexane layer (grey) reduced sample evaporation. (b) Timeline of a typical experiment that collects both mass spectra and flow rate data. (c) Microscopy images of the emitter at three time points. Red arrows indicate the phase boundary between the aqueous sample (right) and hexane (left).

Department of Chemistry, University of New Hampshire, 23 Academic Way, Durham, NH 03824, USA. E-mail: Anyin.Li@unh.edu

†Electronic supplementary information (ESI) available. See DOI: 10.1039/d1an02190g

sealing the sample solution with hexane (Fig. S1†) effectively reduced the evaporation rate to as low as 16 fL min^{-1}.

The relay ESI configuration[18] was adopted to trigger the ionization of ultra-low volume (<10 pL) sample solutions without electrode contact (Fig. 1a and S3†). Previously, it was demonstrated that ESI may be triggered by placing the electrode at a certain distance from the sample solution surface.[6,19] This was attempted by placing a wire electrode in the hexane layer, but no ionization was observed using voltages up to 4 kV (Fig. S4†). This suggests that the hexane layer effectively prevented charge flow inside the emitter. In the case of relay ESI, charge transport through the exterior space[9] was not subjected to interference by the hexane layer. By using a wire-in submicron emitter tip as the primary source, an adjustable current (130 fA–2 nA)[16] may lead to charge deposition onto the secondary emitter without introducing extra volumes of liquid, as the charged droplets were rapidly evaporated[20,21] before reaching the secondary emitter tip.

The consumption of the aqueous sample was indicated by the movement of the hexane–water interface upon continuous monitoring by optical microscopy. Bright-field microscopy was effective in identifying interfaces as small as 1 μm (Fig. S5†). Once the relay ESI was turned off, the solution consumption was due to evaporation *via* the tip opening. When the relay ESI was turned on, the ionization of the sample solution was confirmed by the (>5 times) higher consumption rate than the evaporation rate. Video S1† shows one typical experiment in which the ESI flow rate and background evaporation rate were 450 fL min^{-1} and 37 fL min^{-1}, respectively. In the continuously recorded experiments, evaporation rates of 37, 180, 225, 55, and 870 fL min^{-1} and ESI flow rates of 450, 980, 1100, 4000, and 5980 fL min^{-1} were observed, as shown in Videos S1–S3.† There is a general correlation between the observed evaporation rates and ESI flow rates (Fig. S6†). Both had an ~10-fold range, which is likely caused by the variation of emitter tips. When using a plasma ion source as the charge supply,[9,18] the obtained flow rates also fall within this range. In this work, the submicron emitter tips were heat-pulled and had tip sizes ranging from 30 to 160 nm (Table S2 and Fig. S7†). Nevertheless, these femto and low pico flow rates are the lowest ESI flow rates reported in the literature.

The ionization at femto flow rates was further confirmed by mass spectrometry (MS). Volume measurements at multiple time points were carried out to obtain both ESI flow rates and the corresponding mass spectra. Fig. 1b and c illustrate a typical experiment in which 1–10 pL aqueous sample was loaded into the emitter tip. A microscopy image was taken at this time point (t_0) to measure the initial volume of the sample. From t_0 to t_1, the emitter was mounted onto the relay ESI setup and aligned in front of the mass spectrometer. From t_1 to t_2, femto flow electrospray ionization was triggered, and the produced ions were analyzed by MS. From t_2 to t_3, the emitter was brought to the microscope to measure the sample volume. Lastly, another image was taken at t_4 to measure the evaporation rate under the lab conditions. Assuming the evaporation was constant during t_0–t_5, the electrospray flow rate was calculated by the volume difference between V_0 (at t_0) and V_1 (at t_3) after subtracting the evaporation volumes from t_0 to t_1, and from t_2 to t_3. In the experiments, the electrospray volumes were always >5 times larger than the estimated evaporation volumes. The obtained flow rate range is comparable to that obtained by continuous monitoring (Table S3†). This suggests that the microscope lens (2 mm away) had no significant impact on the relay electrospray ionization.

As shown in Fig. 2a, an ESI flow rate of 425 fL min^{-1} produced an average intensity of 0.361 for the analyte MRFA. Although this intensity is 5–6 orders of magnitude lower than that produced by regular nanoESI, the clear isotope pattern of MRFA (Fig. 2a inset) indicates an adequate amount of analyte ions. The relative intensities of MRFA appeared to be low due to the higher intensities of the background signals ranging from *m*/*z* 100–350. These peaks were also observed when running the experiment using an empty secondary emitter tip (Fig. S8†), suggesting that these peaks are more likely to be from the solution in the primary ion source, or desorbed from the glass surfaces. Slightly higher flow rates of 840 fL min^{-1} and 1057 fL min^{-1} produced higher MRFA intensities in the 1×10^1 to 1×10^2 range (Fig. 2b and c). For the above mass spectra, both TIC and EIC had continuous signals with intensity fluctuations within the same order of magnitude (Fig. S9†).

On the LTQ-XL instrument, this femto to low pico flow ESI produced total ion current (ion counts per second) intensities ranging from 1×10^2 to 1×10^4, positively correlated with the flow rates. In comparison, a conventional nanoESI using the same sample solutions produced TIC intensities in the 1×10^6

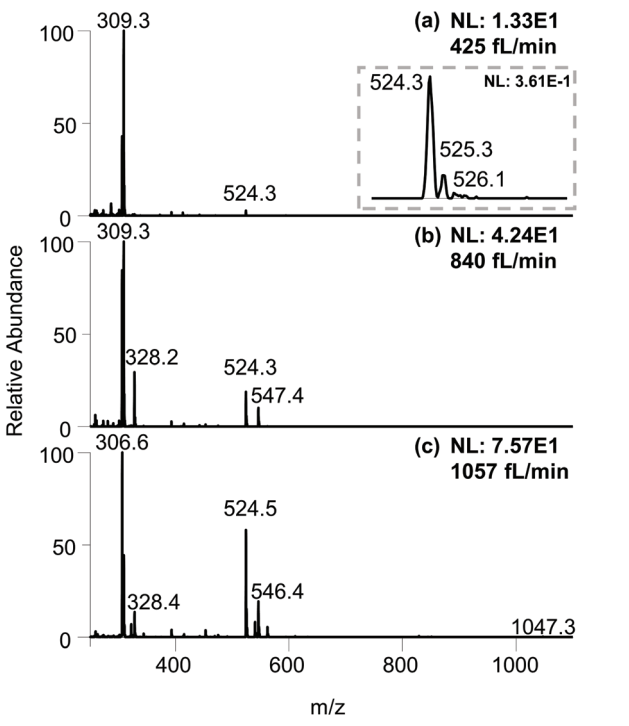

Fig. 2 Full scan mass spectra of 100 μM MRFA at flow rates of (a) 425 fL min^{-1}, (b) 840 fL min^{-1}, and (c) 1057 fL min^{-1}.

to 1×10^7 range (Fig. S9†). The >3 orders of magnitude difference in the total ion current intensities between nanoESI and femto flow ESI makes them easily distinguishable.

The current–voltage characteristics of the whole relay ESI setup were determined (Fig. S10†). The onsets were typically at hundreds of fA and 300 V. At 1000 V, a total current of 218 pA was observed. Because the primary ions in relay ESI are diffusive and some of them may not be deposited onto the secondary emitter, the actual ionization current of the sample solution is lower than the total current, *i.e.*, <218 pA. The ionization current (I_{obs}) and flow rate (V_f) allow the calculation of the average size of initial charged droplets. Assume each initial charged droplet is at 70% of the Rayleigh limit, and imagine t is the average ejection time for each initial charged droplet; then we have

$$I_{obs} \cdot t = 0.7 \cdot Z_r = 0.7 \cdot 8\pi\sqrt{\varepsilon_0 \gamma {R_i}^3} \quad (1)$$

to describe the observed ionization current I_{obs} and the charge on each droplet, where Z_r is the charge on the droplet, R_i is the droplet radius, ε_0 is the permittivity, and γ is the surface tension of the droplet.[22] Similarly,

$$V_f \cdot t = V_d = \frac{4}{3}\pi {R_i}^3 \quad (2)$$

describes the flow rate (V_f) and the volume (V_d) of each droplet. Dividing the first equation by the second, and solving for R_i, the following equation is obtained for the droplet radius:

$$R_i = \sqrt[3]{\frac{(0.7 \times 6)^2 \varepsilon_0 \gamma \cdot {V_f}^2}{{I_{obs}}^2}} \quad (3)$$

Recently, Davidson *et al.* reported <10 nL min^{-1} flow rate and 30 nA ionization current in a nanoESI experiment.[23] When plugging in the flow rate and current, eqn (3) returns a diameter of <140 nm, which is in line with the measured size of 60 nm. In this work, the measured flow rate of 425 fL min^{-1} and a <218 pA ionization current indicates that the initial charged droplets are on average no smaller than 5 nm, which is on a par with the estimated droplet size for submicron emitter tips.[13] With an emitter diameter of 30–160 nm, the ratio of the droplet size to the emitter diameter is 1/6–1/32. This ratio has a wider range than the previously suggested value range of 1/14–1/20,[10,23] which was obtained using a wire-in electrode and emitters with narrower tip size distributions.

Operating submicron emitter tips are known to have practical problems in loading and spraying. One work reported a success rate of 70% for sample loading from the back end.[12] Clogging during electrospray is another common problem. In this work, front-loading through the emitter tip effectively filters out particles larger than the tip opening, which could reduce the chance of clogging. Yet, clogging events were still observed to cause the sudden disappearance of the analyte ion signal. Interestingly, solvent evaporation was not blocked after clogging, suggesting that the tip was partially clogged and it filtered out the analytes (Fig. S11†). When running a protein–peptide mixture solution (MRFA and cytochrome c), similar partial clogging was sometimes observed, eliminating the ion signal of the larger analyte, *i.e.*, cyt c (Fig. S12†). This clogging does not seem to be correlated with the pI value of proteins (Fig. S17†).

When using emitter tips that produced higher flow rates in the low pico flow rate range (1–10 pL min^{-1}), the cyt c signal was readily observed. As shown in Fig. 3a, a flow rate of 7.7 pL min^{-1} produced a signal intensity of 4.8×10^2 for the cyt c peaks. The intensity is analogous to that of the wire-in ESI using a similar submicron emitter tip (Fig. 3b) and is two orders of magnitude lower than that of nanoESI using a micrometer emitter tip (Fig. 3c). In comparison, the flow rate is more than three orders of magnitude lower than that of a typical nanoESI.[9,23] This confirms the improved overall ionization and transmission efficiency at lower flow rates, which aligns with the previous observation with lower current ion beams.[16]

Interestingly, the total ion current intensity produced by fA ESI (Fig. 3d) is generally at least two orders of magnitude (119–481 fold, Fig. S18†) lower than that produced by this 7.7 pL min^{-1} relay ESI. Assuming the overall ionization and transmission efficiency to be similar and slightly enhanced for this

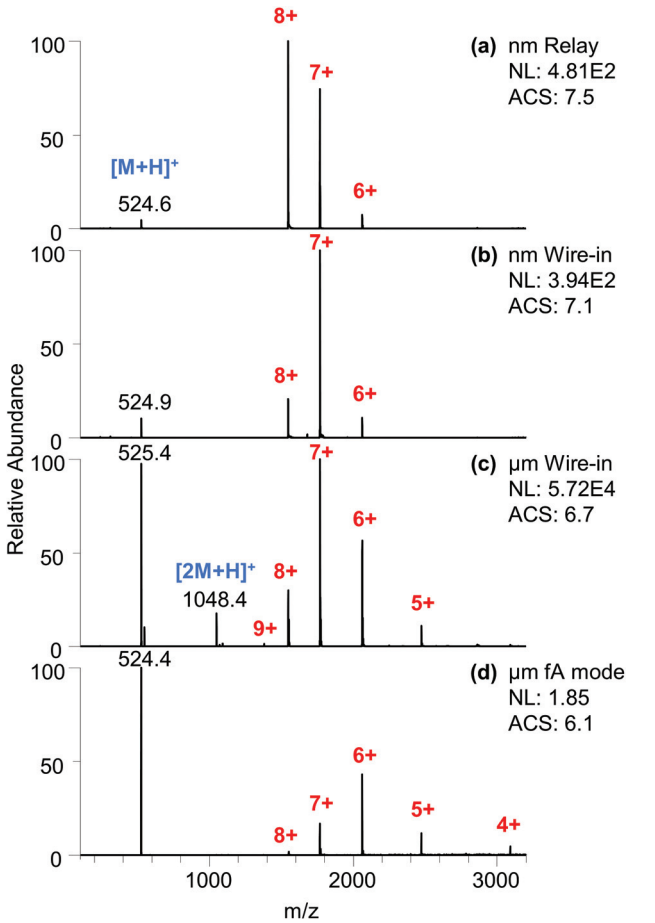

Fig. 3 Full scan mass spectra of a 50 μM cyt c and 50 μM MRFA aqueous mixture under different conditions. (a) Relay ESI using a submicron emitter tip with a 7.7 pL min^{-1} flow rate. (b) Wire-in ESI using a submicron emitter tip. (c) NanoESI using a micrometer emitter tip. (d) fA ESI using a micrometer emitter tip.

lower ion current, the lower limit of the flow rate for fA ESI is 16–65 fL min^{-1}. Using these values and the 400 fA ionization current,[16] eqn (3) returns a droplet size larger than 34–87 nm for the fA ESI. Considering that the hydrodynamic radius in cyt c is 1.7 ± 0.2 nm,[24,25] these sizes suggest the spraying of charged droplets in fA ESI. The postulated direct ion emission[26] from a nanoscale meniscus[27] is possible but it alone would not produce the estimated flow rate.

The charged droplets produced by these low flow ESI methods were evaluated using the charge state pattern of cyt c. The protein solution was prepared without any buffering agent to reveal the altered chemical environments. The submicron emitter tip (both relay ESI and wire-in ESI) produced higher average charge states (7.5 and 7.1, Fig. 3a and b). It is worth noting that these higher charge states are all among the 7+ and 8+ folded charge states. The trend of producing more of the higher charged native states when using a smaller emitter tip (or channel) aligns with previous reports.[4,28] The combination of relay ESI and a submicron emitter has pushed this trend to an extreme. The highly abundant 8+ peak and the lack of 9+ and 10+ peaks produced an oddly asymmetrical pattern that obviously deviates from the typical Gaussian profile patterns produced by ESI. In comparison, a submicron emitter in the wire-in mode produced symmetrical profiles (Fig. 3b). The symmetrical Gaussian-like profile of protein ions is believed to be the result of solution phase pH equilibria.[29] The disappearance of such symmetry suggests that potential gas phase processes are at play. Native cyt c protein has a calculated Rayleigh limit of 8.6.[30] Lower average charge states (ACS 6.8–7.2) were produced due to the loss of the charge carrier by ion emission at a threshold lower than the Rayleigh limit, as described in the combined charge residue and field emission model.[31] The ACS of 7.5 in Fig. 3a with only native peaks indicates that a significant population of the charged droplets has surpassed the threshold for charge carrier emission. In relay ESI,[18] the primary charge not deposited onto the secondary emitter may coexist with the ESI plume. These surrounding extra charges could have suppressed the emission of the charge carrier in the late stage of the ESI droplet, thus squeezing peaks into a narrower distribution of higher charge states, which could enhance the sensitivity for low concentration samples.

In comparison, nanoESI (Fig. 3c) produced an ACS of 6.7 with a symmetrical profile that also contains the partially unfolded 9+ charge states.[32,33] When a higher voltage was applied, higher average charge states and increasing abundances of partially unfolded protein ions (9+, 10+) were observed (Fig. S13†). A similar trend was observed when using a submicron emitter with wire-in configuration (Fig. S14†). The unfolding could be due to multiple factors including pH evolution of the unbuffered charged droplets, increased collision,[34] and heating of larger droplets in the source region.[20] In contrast, the lower native charge states (ACS 6.1) exhibit a charge-reducing[35] effect in fA ESI (Fig. 3d).

Comparing the relative ion intensities of proteins and MRFA, the submicron emitter tips (Fig. 3a and b) produced similarly high ratios of 36 : 1 and 13 : 1 that favor the cyt c protein. NanoESI (Fig. 3c) produced a relatively smaller ratio (1.5 : 1). The fA ESI produced a ratio (0.77 : 1) that is closest to the actual concentration ratio (Fig. 3d). These results indicate that the relative ionization efficiency is very sensitive to experimental parameters, including the flow rate, ionization current, and emitter tip size.

The ionization of other classes of analytes was also measured (Table S3†). For some of them, the ESI flow rate may be calculated using the loaded sample volume and sample depletion time as indicated by MS. For example, a glycan mixture solution of 6.35 pL was consumed in 2.27 minutes by relay ESI, corresponding to a consumption flow rate of 2.8 pL min^{-1} (Fig. S15†). The same emitter recorded a comparable flow rate of 4.5 pL min^{-1} when using the more complicated workflow (Fig. 1b). However, this simplified depletion time approach may not be applicable for those analytes that may adhere to the emitter tip to produce similar signal intensities after the depletion of the sample solution, as can be seen in the cases of amitriptyline and acetylcholine (Fig. S16†).

Conclusions

In summary, femto to low pico flow rate electrospray ionization was measured for the first time. The measured data points could contribute to a better understanding of the low intensity modes of electrospray from a submicron meniscus. Compared with nanoESI, femto flow ESI exhibits lower ion current intensities (>2 orders of magnitude lower), ionization currents <218 pA, and lower flow rates (>3 orders of magnitude lower). These characteristics could serve as indicators for femto flow ionization in experiments when flow rate measurement is not available. The femto flow ionization technique used here enabled the use of highly concentrated sample solutions in regular MS analysis, which suggests it could remove the need for dilution when lower intensity ion beams are needed, such as in charge detection mass spectrometry. In a typical experiment, tens of attomoles per MS scan produced signals above the detection limit. This absolute sensitivity is on a par with conventional ESI and indicates excellent ionization efficiency in femto ESI. For a non-buffered protein solution, the low flow ionization modes allow native charge states to be produced in an either charge-enhancing or charge-reducing manner. The measured flow rates and ionization currents enable the calculation of the size of initial charged nanodroplets.

Author contributions

Huishan Li: investigation, methodology, data curation, formal analysis, writing – original draft, writing – review and editing. Nicholas Allen: investigation, data curation. Mengtian Li: resources. Anyin Li: supervision, conceptualization, methodology, investigation, formal analysis, writing – original draft, writing – review and editing, project administration, funding acquisition.

Conflicts of interest

There are no conflicts of interest to declare.

Acknowledgements

The authors acknowledge the start-up funding from the University of New Hampshire.

Notes and references

1 J. B. Fenn, M. Mann, C. K. Meng, S. F. Wong and C. M. Whitehouse, *Science*, 1989, **246**, 64–71.
2 S. Rauschenbach, F. L. Stadler, E. Lunedei, N. Malinowski, S. Koltsov, G. Costantini and K. Kern, *Small*, 2006, **2**, 540–547.
3 L. deJuan and J. F. delaMora, *J. Colloid Interface Sci.*, 1997, **186**, 280–293.
4 E. M. Yuill, N. Sa, S. J. Ray, G. M. Hieftje and L. A. Baker, *Anal. Chem.*, 2013, **85**, 8498–8502.
5 T. Kenderdine, Z. Xia, E. R. Williams and D. Fabris, *Anal. Chem.*, 2018, **90**, 13541–13548.
6 Z. Wei, X. Xiong, C. Guo, X. Si, Y. Zhao, M. He, C. Yang, W. Xu, F. Tang, X. Fang, S. Zhang and X. Zhang, *Anal. Chem.*, 2015, **87**, 11242–11248.
7 I. Marginean, K. Tang, R. D. Smith and R. T. Kelly, *J. Am. Soc. Mass. Spectrom.*, 2014, **25**, 30–36.
8 G. Huang, G. Li and R. G. Cooks, *Angew. Chem., Int. Ed.*, 2011, **50**, 9907–9910.
9 M. Li, H. Li, N. R. Allen, T. Wang, L. Li, J. Schwartz and A. Li, *Chem. Sci.*, 2021, **12**, 1907–1914.
10 A. C. Susa, Z. Xia and E. R. Williams, *Anal. Chem.*, 2017, **89**, 3116–3122.
11 Z. Xia and E. R. Williams, *J. Am. Soc. Mass. Spectrom.*, 2018, **29**, 194–202.
12 G. T. H. Nguyen, T. N. Tran, M. N. Podgorski, S. G. Bell, C. T. Supuran and W. A. Donald, *ACS Cent. Sci.*, 2019, **5**, 308–318.
13 E. G. B. Bolivar, D. T. Bui, E. N. Kitova, L. Han, R. X. B. Zheng, E. J. Luber, S. Y. Sayed, L. K. Mahal and J. S. Klassen, *Anal. Chem.*, 2021, **93**, 4231–4239.
14 E. M. Panczyk, J. D. Gilbert, G. S. Jagdale, A. Q. Stiving, L. A. Baker and V. H. Wysocki, *Anal. Chem.*, 2020, **92**, 2460–2467.
15 J. Hu, X. X. Jiang, J. Wang, Q. Y. Guan, P. K. Zhang, J. J. Xu and H. Y. Chen, *Anal. Chem.*, 2016, **88**, 7245–7251.
16 N. R. Allen, H. Li, A. Cheung, G. Xu, Y. Zi and A. Li, *Int. J. Mass spectrom.*, 2021, **469**, 116696.
17 M. Li, H. Li, N. R. Allen, T. Wang, L. Li, J. Schwartz and A. Li, *Chem. Sci.*, 2021, **12**(5), 1907–1914.
18 A. Li, A. Hollerbach, Q. Luo and R. G. Cooks, *Angew. Chem., Int. Ed.*, 2015, **54**, 6893–6895.
19 A. J. Schwartz, J. T. Shelley, C. L. Walton, K. L. Williams and G. M. Hieftje, *Chem. Sci.*, 2016, **7**, 6440–6449.
20 Z. J. Xia and E. R. Williams, *Analyst*, 2019, **144**, 237–248.
21 Z. Olumee, J. H. Callahan and A. Vertes, *Anal. Chem.*, 1999, **71**, 4111–4113.
22 L. Rayleigh, *The London, Edinburgh, and Dublin Philosophical Magazine and Journal of Science*, 1882, **14**, 184–186.
23 K. L. Davidson, D. R. Oberreit, C. J. Hogan and M. F. Bush, *Int. J. Mass spectrom.*, 2017, **420**, 35–42.
24 C. Ghosh, M. A. AMIN, B. Jana and K. Bhattacharyya, *J. Chem. Sci.*, 2017, **129**, 841–847.
25 E. Aliyari and L. Konermann, *Anal. Chem.*, 2021, **93**, 12748–12757.
26 B. A. Thomson and J. V. Iribarne, *J. Chem. Phys.*, 1979, **71**, 4451–4463.
27 L. A. Baker and G. S. Jagdale, *Curr. Opin. Electrochem.*, 2019, **13**, 140–146.
28 Y. Li and R. B. Cole, *Anal. Chem.*, 2003, **75**, 5739–5746.
29 R. Guevremont, K. W. M. Siu, J. C. Y. Leblanc and S. S. Berman, *J. Am. Soc. Mass. Spectrom.*, 1992, **3**, 216–224.
30 S. J. Allen, A. M. Schwartz and M. F. Bush, *Anal. Chem.*, 2013, **85**, 12055–12061.
31 C. J. Hogan Jr., J. A. Carroll, H. W. Rohrs, P. Biswas and M. L. Gross, *Anal. Chem.*, 2009, **81**, 369–377.
32 J. K. Lee, S. Kim, H. G. Nam and R. N. Zare, *Proc. Natl. Acad. Sci. U. S. A.*, 2015, **112**, 3898–3903.
33 J. C. May, E. Jurneczko, S. M. Stow, I. Kratochvil, S. Kalkhof and J. A. McLean, *Int. J. Mass spectrom.*, 2018, **427**, 79–90.
34 D. N. Mortensen and E. R. Williams, *Anal. Chem.*, 2016, **88**, 9662–9668.
35 A. Q. Stiving, B. J. Jones, J. Ujma, K. Giles and V. H. Wysocki, *Anal. Chem.*, 2020, **92**, 4475–4483.